Opto-Electronic Science

CN 51-1800/O4 ISSN 2097-0382 (Print) ISSN 2097-4000 (Online)

Recent advances in exciton-polariton in perovskite

Khalil As'ham, Andergachew Mekonnen Berhe, Ibrahim A. M. Al-Ani, Haroldo T. Hattori and Andrey E. Miroshnichenko

Citation: As'ham K, Berhe AM, Al-Ani IAM, et al. Recent advances in exciton-polariton in perovskite. *Opto-Electron Sci* **4**, 250001 (2025).

https://doi.org/10.29026/oes.2025.250001

Received: 10 January 2025; Accepted: 1 April 2025; Published online: 22 August 2025

Related articles

Polariton lasing in Mie-resonant perovskite nanocavity

Mikhail A. Masharin, Daria Khmelevskaia, Valeriy I. Kondratiev, Daria I. Markina, Anton D. Utyushev, Dmitriy M. Dolgintsev, Alexey D. Dmitriev, Vanik A. Shahnazaryan, Anatoly P. Pushkarev, Furkan Isik, Ivan V. Iorsh, et al

Opto-Electronic Advances 2024 **7**, 230148 doi: 10.29026/oea.2024.230148

Enhanced amplified spontaneous emission via splitted strong coupling mode in large-area plasmonic cone lattices

Jiazhi Yuan, Jiang Hu, Yan Zheng, Hao Wei, Jiamin Xiao, Yi Wang, Xuchao Zhao, Ye Xiang, Yong Lei, Wenxin Wang

Opto-Electronic Science 2025 **4**, 240021 doi: 10.29026/oes.2025.240021

Observation of polaronic state assisted sub-bandgap saturable absorption

Li Zhou, Yiduo Wang, Jianlong Kang, Xin Li, Quan Long, Xianming Zhong, Zhihui Chen, Chuanjia Tong, Keqiang Chen, Zi-Lan Deng, Zhengwei Zhang, Chuan-Cun Shu, Yongbo Yuan, Xiang Ni, Si Xiao, Xiangping Li, Yingwei Wang, Jun He

Opto-Electronic Advances 2025 **8**, 240312 doi: 10.29026/oea.2025.240312

Tunable vertical cavity microlasers based on $MAPbI_3$ phase change perovskite

Rongzi Wang, Ying Su, Hongji Fan, Chengxiang Qi, Shuang Zhang, Tun Cao

Opto-Electronic Advances 2025 **8**, 240220 doi: 10.29026/oea.2025.240220

More related article in Opto-Electronic Journals Group website

OES Opto-Electronic Science

http://www.oejournal.org/oes

OE_Journal

Website

Opto-Electronic Science

Review

September 2025, Vol. 4, No. 9

DOI: 10.29026/oes.2025.250001 CSTR: 32246.14.oes.2025.250001

Recent advances in exciton-polariton in perovskite

Khalil As'ham, Andergachew Mekonnen Berhe, Ibrahim A. M. Al-Ani, Haroldo T. Hattori and Andrey E. Miroshnichenko*

Along with being superior in solar cell applications, perovskites are also gaining popularity as an ideal semiconductor material for investigating light-matter interaction in the strong coupling regime. In recent years, the demonstration of exciton-polaritons in perovskites has advanced rapidly due to the materials' exceptional optical characteristics, which include relatively high refractive indices, large binding energies, strong room-temperature excitons, broad wavelength tunability, and simple and cost-effective growth conditions. Here, we discuss the fundamental properties of perovskite semiconductors for exciton-polaritons and review their recent rapid advances in the strong coupling between excitons in perovskite and various photonic cavities. More specifically, we survey the recent progress on the theoretical and experimental realization of strong light-matter interaction using a variety of optical cavities, and their applications in the polariton condensation and polariton lasing. Finally, we provide an outlook and future prospects in this exciting field.

Keywords: perovskites; strong coupling regime; exciton-polariton; Rabi splitting

As'ham K, Berhe AM, Al-Ani IAM et al. Recent advances in exciton-polariton in perovskite. *Opto-Electron Sci* **4**, 250001 (2025).

Introduction

In addition to aiding us in comprehending the world around us in all of its various forms and colours, research into the interaction between light and matter has also made it possible to develop many of the cutting-edge technologies we use today. Light usually interacts with matter in two ways: without energy exchange (no coupling), as in reflection, transmission, and scattering, or with energy exchange (coupling), as in absorption, emission, and strong coupling. Strong coupling between exciton and photonic cavities offers an excellent platform for studying different kinds of fascinating physics phenomena, including Bose-Einstein condensates, polariton bistability, and superfluidity. Furthermore, strong coupling allows for developing several innovative applications and technologies, including ultralow threshold polariton lasing and ultrafast all-optical switch systems[1,2].

Many traditional organic, inorganic, and wideband gap semiconductor materials, such as silicon, gallium arsenide, gallium nitride, and zinc oxide, have been incorporated into various resonant photonic structures to demonstrate strong coupling between light and matter. However, these materials suffer from either the small binding energy of excitons that makes the observation of strong coupling only possible at cryogenic temperature or expensive and complicated fabrication processes. Therefore, it is necessary to develop strong coupling at room temperature cost-effectively. The emergence of transition metal dichalcogenides (TMDC) monolayers have demonstrated huge potential in this regard due to their intriguing physical and chemical properties as well as their large exciton binding energy at room temperature[3,4].

School of Engineering and Technology, University of New South Wales at Canberra, Northcott Drive, Canberra ACT 2610, Australia.
*Correspondence: AE Miroshnichenko, E-mail: andrey.miroshnichenko@unsw.edu.au
Received: 10 January 2025; Accepted: 1 April 2025; Published online: 22 August 2025

Open Access This article is licensed under a Creative Commons Attribution 4.0 International License.
To view a copy of this license, visit http://creativecommons.org/licenses/by/4.0/.

© The Author(s) 2025. Published by Institute of Optics and Electronics, Chinese Academy of Sciences.

These high quality TMDCs, however, are typically produced using low-throughput exfoliation techniques and are typically only micrometre in size.

In contrast, lead halide perovskite materials have a direct bandgap, thus enabling high luminescence quantum yield and making them promising candidates for next-generation photonic devices[5–9]. Furthermore, they have large exciton binding energy, rendering them an ideal platform for realizing exciton-polariton at room temperature[10,11]. In addition to their direct bandgap, perovskites exhibit strong oscillator strength and composition-dependent tunability, allowing precise control of optical properties across a broad spectral range. Their solution-processable nature enables cost-effective and scalable fabrication of high-quality thin films and photonic structures at room temperature, distinguishing them from traditional semiconductors that often require complex and expensive processing. These advantages collectively facilitate robust exciton-photon coupling, leading to enhanced nonlinear phenomena at ambient conditions. Consequently, perovskites provide a versatile and powerful platform for both fundamental studies and practical implementations of strong coupling, outperforming many conventional materials in terms of ease of fabrication and operational temperature range.

This review surveys recent advances in strong coupling observation in lead halide perovskite materials. We first briefly introduce the fundamental physics of strong coupling, followed by a highlight of perovskite optical properties. Then, the strong coupling between excitons in perovskite and mirror-based microcavities is discussed. Following that, we discuss the plasmonic nanostructures approach for strong coupling observation in perovskite materials. Besides, we also review the recent progress on exciton-polariton by leveraging optical resonances in all-dielectric metasurfaces. Finally, we provide our vision of the challenges and opportunities in this rapidly developing field.

Introduction to strong coupling regime

Light-matter interaction falls within the strong coupling regime when the energy exchange rates between light and matter exceed their decoherence rates. This strong coupling, for instance, between excitons in perovskite materials and photonic or plasmonic cavities, can be described by the coupled oscillator model[12–15]:

$$\begin{pmatrix} E_{\rm P}+{\rm i}\hbar\Gamma_{\rm P} & g \\ g & E_{\rm X}+{\rm i}\hbar\Gamma_{\rm X} \end{pmatrix}\begin{pmatrix} \alpha \\ \beta \end{pmatrix}=E_{\rm LP,UP}\begin{pmatrix} \alpha \\ \beta \end{pmatrix}, \tag{1}$$

where $E_{\rm P}$ and $E_{\rm X}$ are the resonance energies of the cavity photon and exciton, respectively; g is the coupling strength, and $\hbar\Gamma_{\rm P}$ and $\hbar\Gamma_{\rm X}$ are the half-widths at half-maximum (HWHM) of the photonic and excitonic resonances. The eigenvalues, $E_{\rm LP,UP}$ are the energies of the resulting mixed states, and α and β are the corresponding eigenvector components satisfying $|\alpha|^2+|\beta|^2=1$. As illustrated in the energy diagram in Fig. 1(a), these mixed states form two distinct energy branches: the upper polariton (UP) and the lower polariton (LP) branches.

Taking the determinant of Eq. (1) leads to the expression for $E_{\rm LP,UP}$:

$$E_{\rm LP,UP}=\frac{1}{2}[(E_{\rm X}+E_{\rm P}])+{\rm i}(\hbar\Gamma_{\rm X}+\hbar\Gamma_{\rm P})] \pm\sqrt{g^2-\frac{1}{4}[E_{\rm X}-E_{\rm P}+{\rm i}\,(\hbar\Gamma_{\rm X}-\hbar\Gamma_{\rm P})]^2}\,. \tag{2}$$

The coupling strength can be reflected by Rabi splitting energy ($\hbar\Omega$), which is the minimum energy difference between the two branches. When $E_{\rm P}=E_{\rm X}$, the Rabi splitting becomes:

$$\hbar\Omega=2\sqrt{g^2-\frac{1}{4}\,(\hbar\Gamma_{\rm X}-\hbar\Gamma_{\rm P})^2}\,. \tag{3}$$

Therefore, to realize exciton-polaritons in perovskites, two conditions must be satisfied: $g>\dfrac{|\hbar\Gamma_{\rm P}-\hbar\Gamma_{\rm X}|}{2}$, and $g>\sqrt{\dfrac{1}{2}(\hbar\Gamma_{\rm P})^2+\dfrac{1}{2}(\hbar\Gamma_{\rm X})^2}$. When these conditions are met, the system enters the strong coupling regime. In this regime, photons emitted after the recombination of an electron and the hole will not propagate away; instead, the system will absorb it again, leading to energy exchange back and forth between the photon and exciton. The uniqueness of such mixed states lies in the combined advantages of their photonic and excitonic parts, which promise many novel applications in photonics, information processing and quantum technologies[16,17].

In addition to the above theoretical explanation, a system entering the strong coupling regime can be clearly identified experimentally by the existence of two peaks in the absorption and photoluminescence (PL) spectra that correspond to the formation of the two polaritons branches (Fig. 1(a)). Another feature of a strongly coupled system is the anti-crossing behavior in dispersion curves of the resonances when the cavity resonance is detuned around the exciton resonance (Fig. 1(b)).

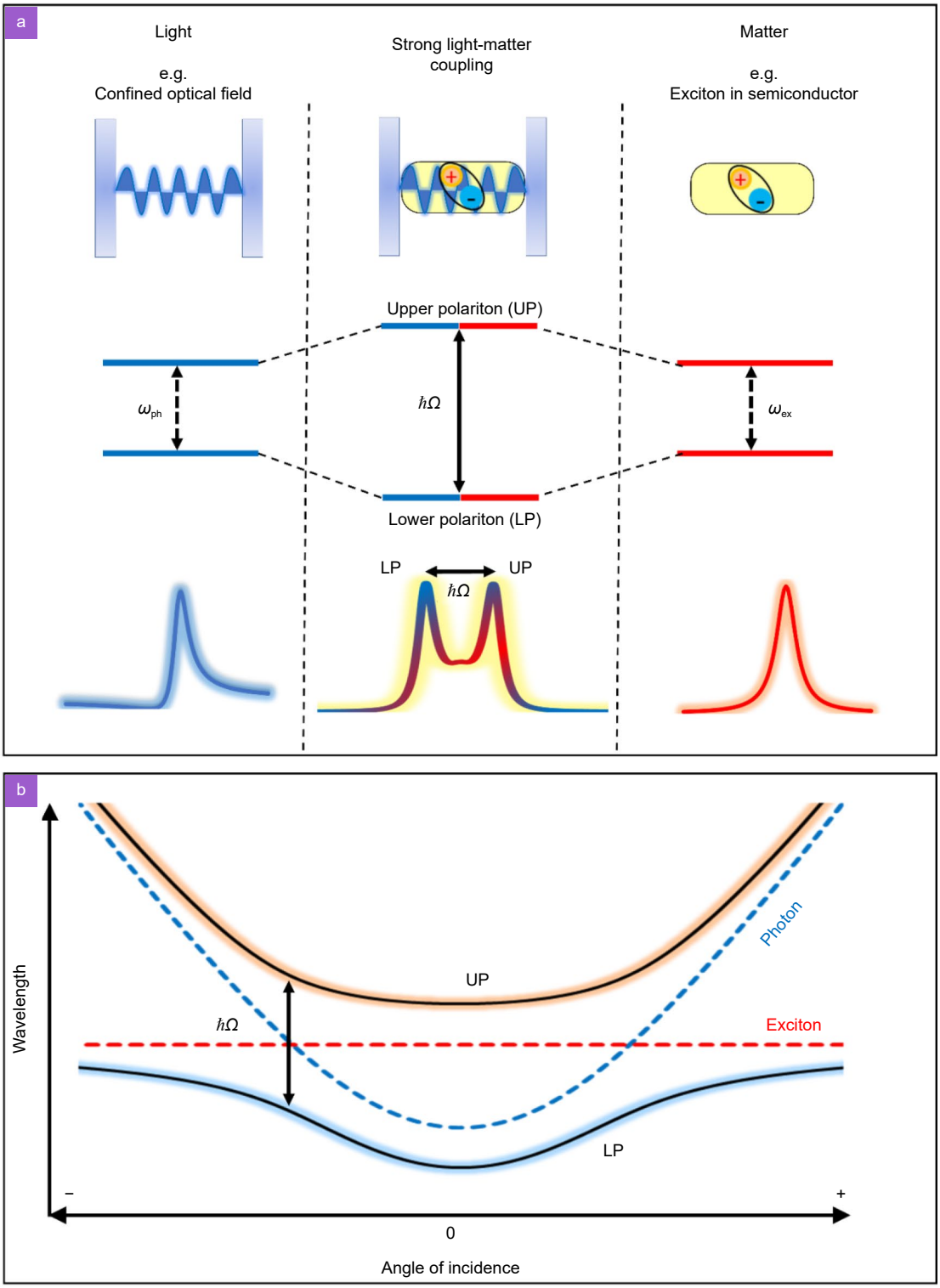


Fig. 1 | Schematic illustration of light-matter interaction in the strong coupling regime. (**a**) Schematic representation of strong coupling between a cavity mode and an exciton in a semiconductor leading to energy spilt into two branches as shown in energy diagram and absorption spectrum. (**b**) Anti-crossing behavior of light (Photonic mode) and matter (Exciton) when the cavity resonance is detuned around the exciton resonance.

The formed mixed state has the combined advantages of the photonic part, such as rapid propagation and low effective mass, as well as the highly desirable optical properties of exciton, such as nonlinearity. These joint properties not only provide an ideal platform for studying many compelling physics phenomena such as Bose-

Einstein condensation, polariton bistability, and superfluidity, but also lead to the emergence of many novel applications and technologies such as ultra-small polariton laser[18], ultrafast all-optical switching[19,20], and transfer technologies. In addition, it exhibits considerable potential for high-performance all-optical 2D devices.

Fundamental physics of perovskite semiconductors for exciton-polaritons

In addition to their superiority in solar cell applications, lead halide perovskites are becoming increasingly attractive as a semiconductor material for photodetectors and light-emitting devices such as LEDs and microlasers. They have a high absorption coefficient, a long diffusion length, a large defect tolerance, and low nonradiative recombination rates. Lead-halide perovskites have the chemical formula ABX_3, where A is a monovalent organic or inorganic cation (Cs^+, Rb^+, $CH_3NH_3^+$, $NH_2CHNH_2^+$, etc.), B is a metal cation (Pb^{2+}, Sn^{2+}, Ge^{2+}, etc.), and X is a halide anion (Cl^-, Br^-, I^-, or their mixture). A schematic illustration of perovskite structures is shown in Fig. 2(a)[21]. As shown in the figure, the 2D Ruddlesden-Popper can be viewed as a stacked structure made of one or more layers of metal-halide octahedra separated by organic cations. This structure is subject to both dielectric and quantum confinement. However, when the number of layers is increased to infinity and confinement is lost, the structure is classified as a 3D bulk perovskite. In the case of a 2D structure, exceptional tunability that is not possible with standard semiconductor materials could be achieved by changing the cations or anions, the number of inorganic layers, or the organic

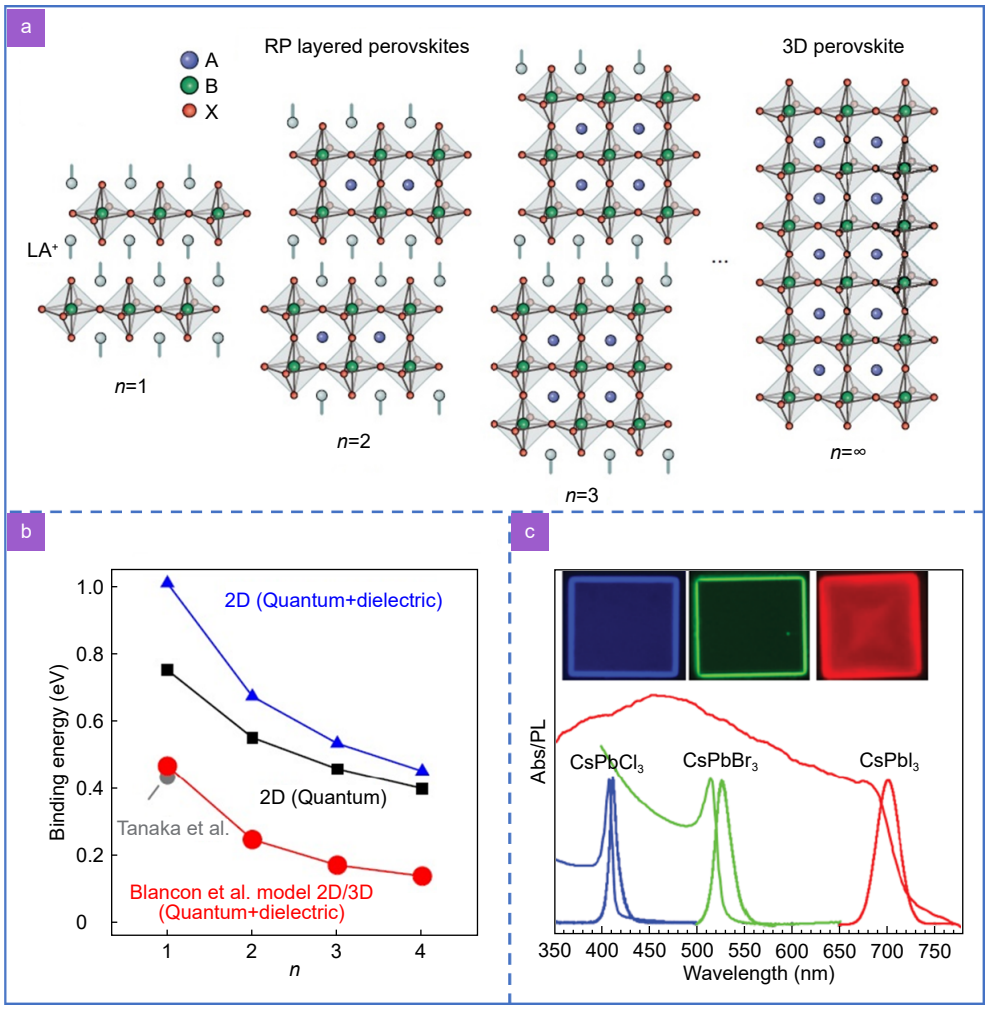


Fig. 2 | Optical properties of perovskite. (**a**) Crystal structures of metal halide perovskites. (**b**) The exciton ground state's binding energy of perovskite decreases with the increase in the inorganic layer number because of weak quantum confinement at high inorganic layer numbers. (**c**) Shows $CsPbCl_3$, $CsPbBr_3$, and $CsPbI_3$ nanoplatelet optical absorption and PL spectra. Figure reproduced with permission from: (a) ref.[21], Springer Nature; (b) ref.[25], under a Creative Commons Attribution License; (c) ref.[26], John Wiley and Sons.

portion's characteristics.

Because of their reduced dimensionality and strong confinement, 2D perovskites exhibit significantly higher exciton binding energies compared to their 3D counterparts (typically tens of meV)[22]. This large exciton binding energy not only ensures stable excitons at room temperature but also enhances strong light–matter interactions, a prerequisite for robust exciton-polariton formation in optical cavities. In contrast, while 3D perovskites have lower exciton binding energies, they can still achieve strong coupling due to their high oscillator strengths and ability to form high-quality cavities. For example, Paul Bouteyre et al. demonstrated room-temperature cavity polaritons with 3D hybrid perovskites, achieving a Rabi splitting of 70 meV in a planar microcavity containing a spin-coated $CH_3NH_3PbBr_3$ thin film. These findings underscore the versatility of perovskite materials in exciton-polariton applications[23]. The Ruddlesden-Popper phase in 2D perovskites can further enhance polariton effects due to the large dielectric contrast and quantum confinement, leading to larger Rabi splittings[24].

This adaptability significantly impacts the perovskite material's bandgap and exciton binding energy, as illustrated in Fig. 2(b)[25]. As a result, 2D perovskites show unprecedented control over optical absorption and colorful light emission. Figure 2(c) shows the optical absorption and PL spectra of nanoplatelets composed of $CsPbCl_3$, $CsPbBr_3$, and $CsPbI_3$[26]. Because of these exceptional properties, as well as their low fabrication cost, high refractive indices, and ease of integration with other types of structures, halide perovskites have promised many exciting applications in advanced nanophotonic devices. For instance, Laura Polimeno et al. have demonstrated polariton condensation at room temperature in cesium lead bromide ($CsPbBr_3$) microplatelets, facilitated by whispering gallery modes (WGMs). This was achieved by synthesizing $CsPbBr_3$ microplatelets with controlled geometry using a low-cost capillary bridge method. The precise geometry and high optical quality of these microplatelets enabled the formation of polariton condensates at low excitation thresholds (≈8 μJ/cm²)[27]. This work highlights the critical role of structural engineering in achieving the strong-coupling regime. These unique properties such as low excitation thresholds and ultrafast dynamics can be harnessed to develop more efficient optoelectronic devices, including polariton lasers, high-speed optical communications, and other technologies that require efficient light-matter interactions at room temperature.

Exciton-polaritons in perovskite semiconductors

Strong coupling in Perovskite enabled mirror based microcavities

After the first demonstrations of exciton-polariton in perovskite materials using distributed feedback cavity in 1989[28] and infiltrated photonic crystals in 2001[29], the field was initially driven by the need to establish fundamental light–matter interactions in these emerging materials. Fabry-Pérot based microcavities were proposed as promising candidates for such demonstration mainly owing to their relatively high *Q*-factors. From 2006 to 2012, Fabry-Pérot type microcavities based on all-dielectric mirrors, all-metal mirrors, and hybrid dielectric-metal mirrors have been utilized to realize the strong coupling in 2D-perovskite semiconductor material in several studies[30–36]. These works were interconnected by their shared goal to understand how different cavity architectures could improve exciton-photon coupling, thereby bridging early demonstrations with more refined, application-oriented designs. Later in 2017, both strong coupling and polariton lasing were experimentally realized in a microcavity-based design consisting of all-inorganic perovskite ($CsPbCl_3$) nanoplatelets sandwiched between two distributed Bragg reflectors (DBR) mirrors formed by HfO_2/SiO_2 layers[37]. This advancement not only validated the theoretical predictions but also provided a link between fundamental studies and practical device implementations, as clearly depicted by the schematic in Fig. 3(a) and the experimental data in Fig. 3(b). As a result, Fig. 3(b) reveals the measured absorption and photoluminescence emission of $CsPbCl_3$ perovskite on mica substrate, as well as the polariton emission after the $CsPbCl_3$ perovskite was placed in the microcavity. In 2018, DBR-based microcavities composted of tantalum oxide (Ta_2O_5) and silicon dioxide (SiO_2) were also used to realise the strong coupling large with Rabi splitting (~242 meV) in organic-inorganic perovskite [$(PEA)_2PbI_4$, $(PEA)_2PbBr_4$] at room temperature[38]. The angle-resolved spectroscopy analysis reveals that the hybridized polariton states form coherent and reversible energy oscillations, highlighting the potential of 2D perovskites in exploring quantum phenomena, such as Bose-Einstein condensation.

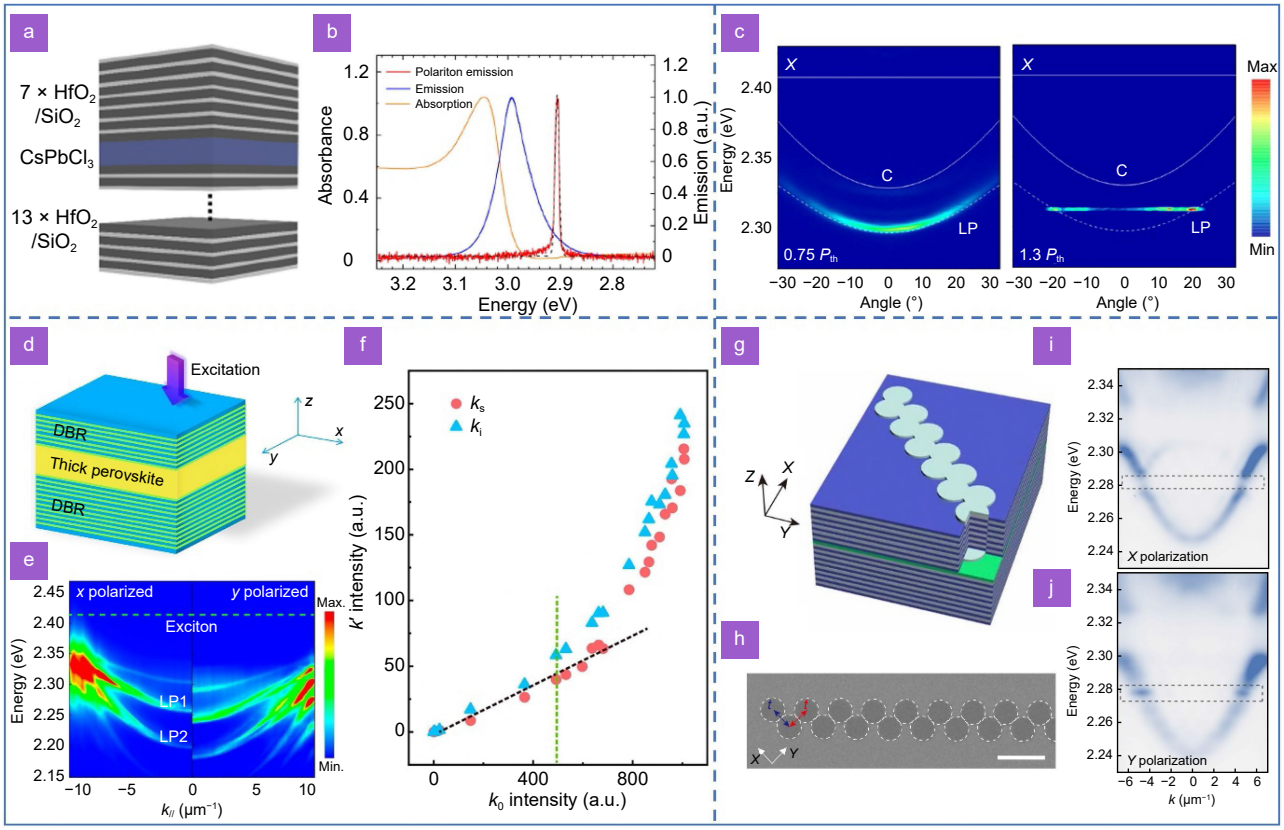


Fig. 3 | Strong coupling in perovskite using mirror-based microcavities. (**a**) A $CsPbCl_3$ crystalline nanoplatelet is placed in a planar microcavity made by a bottom and a top HfO_2/SiO_2 DBRs. (**b**) The room-temperature absorption spectrum and photoluminescence emission spectrum of the $CsPbCl_3$ perovskite nanoplatelet on mica substrate are shown as orange and blue traces, respectively. The red and black dashed traces represent the polariton emission and Gaussian fitting of the $CsPbCl_3$ nanoplatelet embedded in the microcavity. (**c**) Polariton dispersion at 0.75 P_{th} is depicted in the left panel, with a wide distribution visible from all sides. Polariton dispersion at 1.3 P_{th} in the right panel, with symmetric dominant emission at about ±20°. (**d**) The $CsPbBr_3$ perovskite microcavity's schematic diagram. (**e**) Shows multiple polariton modes in the angle-resolved photoluminescence spectral mappings of the $CsPbBr_3$ microcavity along *x* and *y* polarizations under CW excitation; the uncoupled exciton mode is indicated by the green horizontal dashed line. (**f**) Polariton parametric scattering process is indicated by the shift in the intensity dependence between the idler(k_s)/signal(k_i) and the ground state condensate from linear to superlinear behaviour. The green vertical line indicates the threshold for polariton parametric scattering from branch LP_1 to branch LP_2. (**g**) Perovskite zigzag lattice schematic diagram. (**h**) The zigzag chain on the perovskite layer as seen in a scanning electron microscope image. (**i**, **j**) Show the *X* and *Y* polarizations of polariton dispersions as a function of the angle of incidence for the perovskite zigzag lattices, respectively. The grey dashed lines highlight the topological gap that is developing inside the s band. Topological polariton edge states exist within the topological gap in *Y* polarisation. Figure reproduced with permission from: (a, b) ref.[37], American Chemical Society; (c) ref.[39], under a Creative Commons Attribution NonCommercial License; (d–f) ref.[44], American Chemical Society; (g–j) ref.[19], under a Creative Commons Attribution NonCommercial License.

In the same year of 2018, coherent polariton condensate in a one-dimensional all-inorganic cesium lead bromide ($CsPbBr_3$) perovskite microwire embedded into microcavity was experimentally reported for the first time[39]. This pioneering demonstration establishes a critical milestone by achieving robust room-temperature operation and introduces a unique 1D confinement that facilitates long-range coherent propagation. To enter the nonlinear regime, the system was non-resonantly pumped by a 400 nm pulsed laser with a repetition rate of 1 kHz. Such an excitation scheme enables efficient polariton-reservoir interactions, ensuring a rapid build-up of polariton density essential for condensation. Figure 3(c) shows the lower polariton dispersion as a function of the angle of incidence at 0.75 P_{th} and 1.3 P_{th} pumping power (P_{th} = 0.8 mJ/cm^2). The dispersion mapping vividly reveals the transition from a diffuse angular distribution to a highly directional emission pattern, underscoring the system's entry into the nonlinear regime. At 0.75 P_{th}, a broad distribution at all angles is observed, whereas

at 1.3 P_{th}, symmetric dominant emission at around 20° is obtained, indicating the presence of polariton condensates. This marked evolution in emission not only confirms the formation of a coherent condensate but also highlights the device's potential for future applications in all-optical integrated photonic circuits.

One year later, Rydberg exciton polaritons (REPs) that exhibit strong nonlinear behaviour were realized from an excited state in a single crystal $CsPbBr_3$ perovskite strongly coupled to a microcavity based on hybrid metal-dielectric mirrors. These REPs form naturally, exhibiting strong dipole-dipole interactions and a prominent blue shift, attributed to the perovskite's orthorhombic crystal structure. This discovery opens new possibilities for solid-state quantum optical applications, including quantum information processing via correlated photonic states and room-temperature nonlinear optics for ultrafast all-optical switches and low-threshold polariton lasers for next-generation photonic devices[40].

In the same year, another research group has shown that large single-crystal flakes of phenethylammonium lead iodide $(C_6H_5(CH_2)_2NH_3)_2PbI_4$ (PEAI) can sustain strong polariton nonlinearities at room temperature by embedding it into a microcavity based on two DBR mirrors and without an optical cavity formed by highly reflecting mirrors[41]. The study revealed that exciton-exciton interaction energies in these perovskites are spin-dependent and comparable to those observed in inorganic quantum wells (QWs) at cryogenic temperatures. Later, Rui Su et al. have experimentally demonstrated non-equilibrium exciton-polariton condensation using a one-dimensional micropillar array connected by channels in a caesium lead bromide ($CsPbBr_3$) perovskite sandwiched between two DBR mirrors[42]. This configuration resulted in a large forbidden bandgap of up to 13.3 meV and a lattice band width of up to 8.5 meV, significantly surpassing previous systems. This advancement opens avenues for implementing polariton condensates in quantum simulators operable at ambient conditions. Shortly after, both lasing from the bi-exciton state and the subsequent generation of a polariton condensate have been reported in PEAI 2D-perovskite flake placed in a microcavity[43]. This lasing process contributed to the population of the lower polariton branch. At higher excitation powers, a second threshold was surpassed, resulting in the formation of a polariton condensate.

In an exciton-polariton system made of lead halide perovskite ($CsPbBr_3$) and a microcavity constructed from two DBR mirrors, Wu JQ et al[44]. have reported on theoretical and experimental observations of nonlinear parametric scattering, as shown in Fig. 3(d). After exciting the system with a 473 nm continuous-wave (CW) laser, they first achieved several lower polariton modes by strongly coupling the perovskite exciton to multiple cavity photon modes. Figure 3(e) depicts the experimental data of the system's PL spectra mapping as a function of the angle of incidence along x and y polarisations. The mapping data clearly shows lower polariton modes 1 and 2. They then observed a transition from the Rayleigh scattering regime to the nonlinear parametric scattering regime after triggering the polariton condensation with a 400 nm pulsed laser and analysing the power-dependent angle-resolved emission spectra above the condensation threshold. This transformation is evidenced by the change from linear to superlinear behaviour in the intensity dependency between the idler/signal and the ground state condensate, as seen in Fig. 3(f). Such a finding of the parametric scattering effect indicates the onset of room temperature perovskite-based nonlinear polaritonic devices.

In another report, at room temperature, an exciton-polariton topological insulator has been clearly shown to exist in a perovskite zigzag chain inserted in a microcavity[19]. Figure 3(g, h) shows the schematic drawing of the system and SEM image of the zigzag chain on the perovskite layer. By exiting the zigzag chain with a 475 nm CW laser, the authors obtained the energy-resolved momentum-space polariton dispersions from the edge of the perovskite zigzag lattice. Figure 3(i, j) shows the experimental data of the energy-resolved momentum-space PL spectra mapping for X and Y polarizations, respectively. It can be seen that for Y polarization, discrete states emerged inside the topological gap, which correspond to the formation of topological polariton edge states. The emergence of such states is attributed to the anisotropy and strong photonic spin-orbit coupling of halide perovskite microcavities. In the meantime, it allows distinct topological phase switching between the topologically nontrivial and topologically trivial phases by means of polarization switching. Such exciton-polaritons in topological perovskite materials are also crucial for implementing low-power consumption lasers compared with conventional topological lasers that rely on population inversion[45].

The demonstration of strong coupling in perovskite mirror-based microcavities has been further refined

experimentally. For instance, a room-temperature polaritonic *XY* spin Hamiltonian was realized in halide perovskites within a microcavity[46]. The authors used a solution-based nanoconfinement growth approach to create smooth and uniform single-crystalline large crystals required to observe *XY* Hamiltonian lattices at room temperature. First, two DBR mirrors were thermally pressed together with pre-patterned gold pillars acting as spacers, resulting in a symmetric, two-dimensional (2D) limited nanocavity that functions as both the optical cavity and the environment for crystal growth. The halide perovskite solution is then introduced into the system, resulting in excellent quality and large-area yet nanoscale-thickness crystal formation in the gap between the mirrors. *XY* Hamiltonian lattices with sizes up to 10 by 10 were created utilising this synthesis approach. Perovskites are further proven to be a viable material for polaritonic physics at ambient temperature in this experiment.

Additionally, Wang TT et al. have reported the first demonstration of an electrically-injected light-emitting device (LED) based on exciton-polariton in halide perovskite[47]. The proposed LED is made of inorganic perovskite $CsPbBr_3$ microplates sandwiched between few-layer graphite (FLG), hexagonal boron nitride (h-BN), and DBR mirrors at the bottom and h-BN and thin silver mirrors at the top as shown in Fig. 4(a). In addition to being a mirror, the transferred silver layer also serves as an electrode in this design. An alternating current (AC) voltage can be used to inject electrons and holes into the $CsPbBr_3$ microplates separately. Both angle-resolved PL mapping, obtained by exciting the system with a CW laser centred at 405 nm (left panel in Fig. 4(b)), and angle-resolved EL mapping, obtained by applying a bipolar square voltage with a V_{bias} of 20 V and a frequency of 1 MHz (right panel in Fig. 4(b)), provide evidence for the presence of polariton emission. Additionally, as shown in Fig. 4(c), the polariton EL intensity increases with applied voltage, corresponding to enhanced carrier injection at higher voltages. This study paves the way for developing functional perovskite polaritonic devices such as inversion-less electrically pumped lasers and ultrafast light-emitting devices for data transmission.

Moreover, embedding them into optical cavities can also demonstrate strong light-matter coupling in perovskite quantum dots. As a result, Clara Bujalance et al. have achieved strong coupling at room temperature by integrating cesium lead bromide quantum dot ($CsPbBr_3$-QD) solids in silver-based optical cavities. The demonstrated $CsPbBr_3$-QD-based strong coupling has significant implications for reducing photoemission line width and enabling ultrafast modulation of the optical absorption of the QDs[48]. These results pave the way for developing perovskite quantum dot (PQD)-based polaritonic devices.

More recently, Zou C et al. demonstrated room-temperature CW perovskite polariton lasers with remarkably low thresholds, enabled by a variable single-crystal perovskite microcavity (see Fig. 4(d) for the design)[49]. As shown in Fig. 4(e), the lasing properties of these microcavities were investigated using a 405 nm CW diode laser for off-resonant pumping. When the excitation intensity exceeds ~0.4 $W{\cdot}cm^{-2}$, the emission peak at ~551 nm rises sharply, signaling the onset of lasing. The steady-state polariton condensation responsible for this ultralow-threshold lasing is further confirmed through angle-resolved emission measurements at room temperature, as depicted in Fig. 4(f) for the above-threshold condition. As the pumping intensity reaches the threshold, polaritons accumulate at the bottom of the lower polariton (LP) dispersion, a key characteristic that distinguishes polariton condensation from conventional photon lasing. This transition underscores the presence of strong exciton-photon coupling, which plays a crucial role in reducing the lasing threshold. Moreover, the study demonstrates an innovative, indirectly injected perovskite laser chip powered by a GaN LED, which highlights the practical integration potential of these polaritonic devices for on-chip photonic applications. These findings open exciting new avenues for the on-chip integration of solution-processed lasers, offering opportunities for ultralow-energy consumption and high-performance lasing in compact photonic devices.

Additionally, Song JP et al. demonstrated room-temperature CW pumped exciton-polariton condensation in a perovskite microcavity, achieving an exceptionally low condensation threshold of ~0.53 W cm^{-2} [50]. The presence of strong exciton-photon coupling was confirmed through angle-resolved photoluminescence (PL) and reflectance measurements, which exhibited clear anti-crossing behavior with a large Rabi splitting of ~128 meV (Fig. 4(g)). This strong coupling ensures efficient polariton interactions and energy relaxation, facilitating condensation at significantly lower pump powers. As shown in Fig. 4(h), at low pump densities, the lower polariton (LP) branch exhibits a broad angular emission

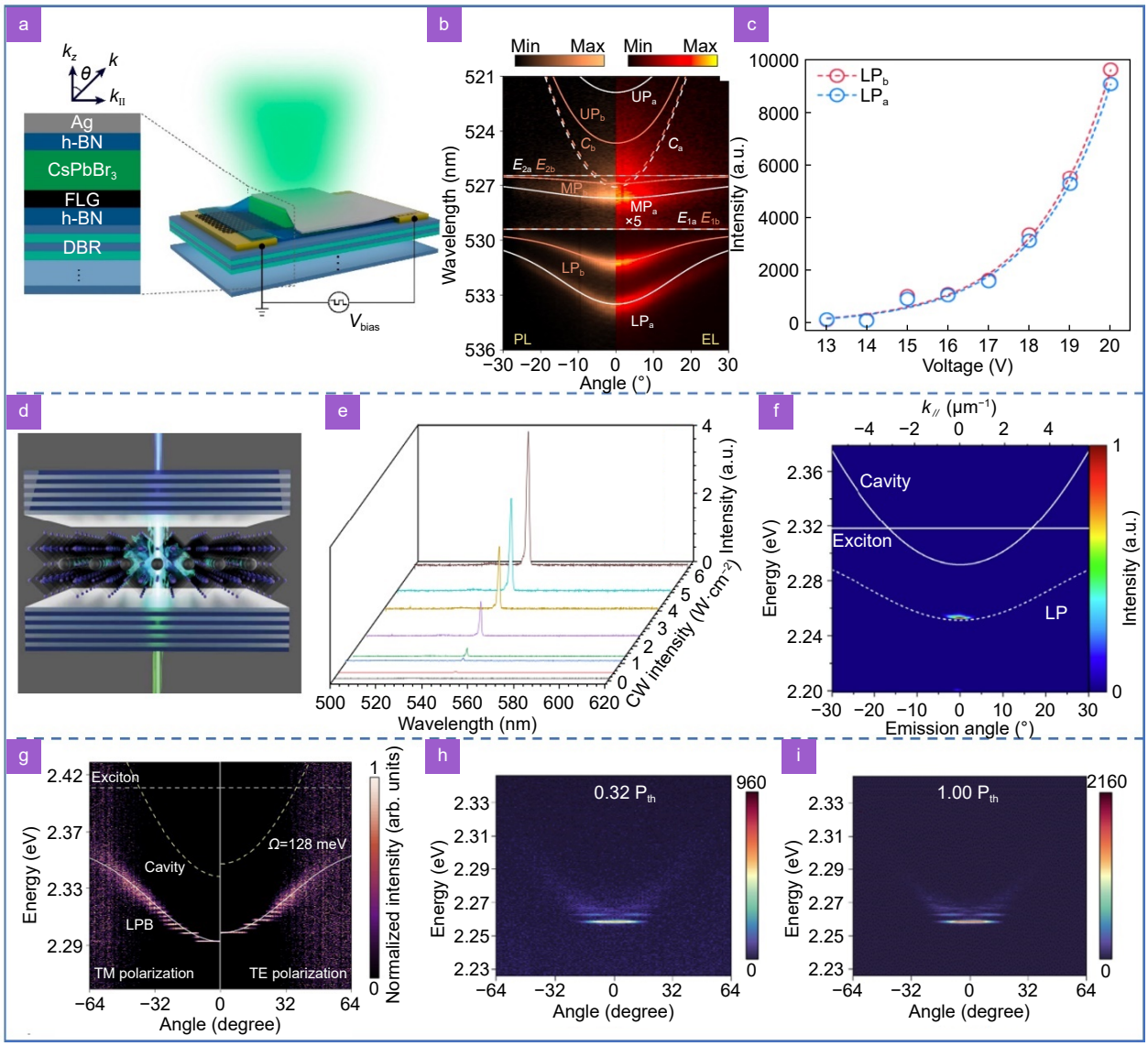


Fig. 4 | Applications of exciton-polariton in perovskite-microcavities hybrid structures. (**a**) The structure of the completed device is presented schematically with the cross-sectional view provided in the inset. (**b**) Maps showing the device's PL (left panel) and EL (right panel), both measured at 7 K. The vertical axis indicates the wavelength, while the horizontal axis is the emission's angle with respect to the *z*-axis. (**c**) Effect of applied voltage on the polariton EL intensity. (**d**) A perovskite single crystal is enclosed between two highly reflective DBRs, enabling CW lasing through strong light-matter interactions. (**e**) Evolution of emission spectra under CW operation by varying pump intensities. (**f**) Angle-resolved PL spectra above the lasing threshold (3.0 P_{th}). The solid straight line represents the dispersion relation of excitons, while the solid parabolic curve corresponds to the dispersion relation of cavity photons. The dashed curve illustrates the dispersion of the lower polariton branch. (**g**) Angle- and polarization-resolved PL spectra of a $CsPbBr_3$ microcavity at room temperature, under nonresonant CW excitation, with the pump density slightly exceeding P_{th}. Lower polariton modes are fitted using the coupled harmonic oscillator model, revealing a Rabi splitting of ~128 meV. Angle-resolved PL spectra under nonresonant CW excitation at pump densities of (**h**) 0.3 P_{th} and (**i**) 1.0 P_{th}. Figure reproduced with permission from: (a–c) ref.[47], American Chemical Society; (d–f) ref.[49], (g, h) ref.[50], under a Creative Commons Attribution NonCommercial License.

distribution, indicating a non-condensed polariton state. However, as the pump density increases to the condensation threshold, a macroscopic occupation of the LP ground state emerges. This transition is characterized by a sudden nonlinear increase in emission intensity and a linewidth narrowing to ~0.5 meV, as depicted in Fig. 4(h, i). These distinct spectral features confirm the onset of steady-state polariton condensation under CW optical excitation at room temperature, distinguishing it from conventional photon lasing. The demonstration of CW polariton condensation in a solution-processed perovskite microcavity represents a significant milestone

in the development of scalable, low-threshold, and miniaturized optical technologies.

In condensed matter, a variety of spintronic and topological phenomena are driven by spin-orbit coupling (SOC). Recently, in microcavities made of birefringent lead halide perovskite single crystals and DBR mirrors, a research group demonstrated photonic analogues of SOCs in exciton-polaritons and associated condensates[51]. They have shown exciton-polaritons with pseudospin textures phase transition to competing condensates with orthogonal polarizations as density rises. Because exciton-polaritons and condensates inherit nonlinearity from their excitonic components, such designs have the potential to serve as quantum simulators for many-body SOC processes.

Strong coupling in perovskite enabled by plasmonic nanostructures

Reducing the mode volume and enhancing the field localisation through the use of plasmonic nanostructures is another method for boosting the coupling between light and matter from weak to strong coupling. The surface plasmon can confine optical modes to subwavelength scales, resulting in extreme localised electromagnetic fields. One of the first studies that employed plasmonic nanostructures to demonstrate strong coupling regime in perovskites was reported in 2015[52]. Wendy Niu et al. used perovskite-coated silver gratings to strongly couple surface plasmon polaritons (SPPs) with the exciton and its image "biexciton," achieving Rabi-splitting of 150 meV and 125 meV. The interaction between excitons and their images in the metallic mirror on which they sit causes the excitation of such biexciton.

In 2018, a substantial Rabi-splitting of 564 meV was recorded in perovskite nanowires strongly coupled to surface plasmons at ambient temperature[53]. The authors employed a $MAPbBr_3$ NW sitting on a SiO_2/Ag substrate with a SiO_2 spacer layer for the strong coupling experiments, as illustrated schematically in Fig. 5(a). In this case, in addition to the surface plasmon given by the metal component, the perovskite naturally works as a Fabry-Pérot microcavity since its two end facets serve as micro-reflectors. Figure 5(b) depicts the polariton dispersion as a function of the wavevector in the z-direction for a perovskite nanowire on top of a glass substrate (pink data points) with a Rabi-splitting of 392 meV and a SiO_2/Ag substrate (navy data points) with a Rabi-splitting of 564 meV, respectively. The enhancement in coupling strength is primarily attributed to the redistribution and localization of the electromagnetic field induced by surface plasmons. This effect arises due to the strong interaction between incident photons and free electrons at the silver-dielectric interface, leading to intense near-field confinement. Moreover, the small skin depth of metals (such as silver), results in a higher degree of field confinement[12].

Another study has theoretically described how exciton-surface plasmon and exciton-photon polaritons can be obtained in a perovskite-based subwavelength lattice on a metallic plane[54]. Using a perovskite thin film deposited on a metallic substrate, two types of guided modes are excited. The first is the dielectric-guided mode (DGM), which occurs within the perovskite layer of wavelength-scale thickness and can be observed in both TE and TM polarizations. The second is the surface plasmon polariton (SPP), located at the perovskite–metal interface and observable only in TM polarization. The top panel of Fig. 5(c) depicts the angle-resolved reflectivity spectra of the passive structure under TM-polarization excitation, revealing both photonic and SPP modes. In the active structure, both exciton-photon and exciton-surface plasmon polaritons are realized with Rabi splittings of $\hbar\Omega_{R1}$ = 241 meV, $\hbar\Omega_{R2}$ = 207 meV, respectively.

Plasmon-polariton-based all-inorganic lead halide perovskite nanocrystals formation in the strong coupling regime has been demonstrated experimentally and theoretically in a recent study[55]. By synthesising nanocrystals with various morphologies, such as nanoplatelets and nanowires, or by altering the halide content in the nanocrystals, the optical characteristics of perovskites have been modified. Then, by exciting the system with a p-polarized, tunable laser, surface plasmon polaritons are produced in the system by placing the perovskite nanocrystals near a chemically functionalized metal sheet in a Kretschmann configuration (as illustrated in Fig. 5(d)). According to the obtained theoretical and experimental reflection mapping data as a function of the angle of incidence, the maximum Rabi splitting was achieved in $CsPbI_3$ nanoplatelets, as displayed in Fig. 5(e, f); these findings further support the notion that perovskite nanocrystals are promising and strong candidates for investigating light-matter interactions at the nanoscale level.

More recently, a plasmonic nanoparticle Al lattice was also connected to 2D Ruddlesden-Popper perovskites for the strong coupling realisation[56]. The proposed plasmon-

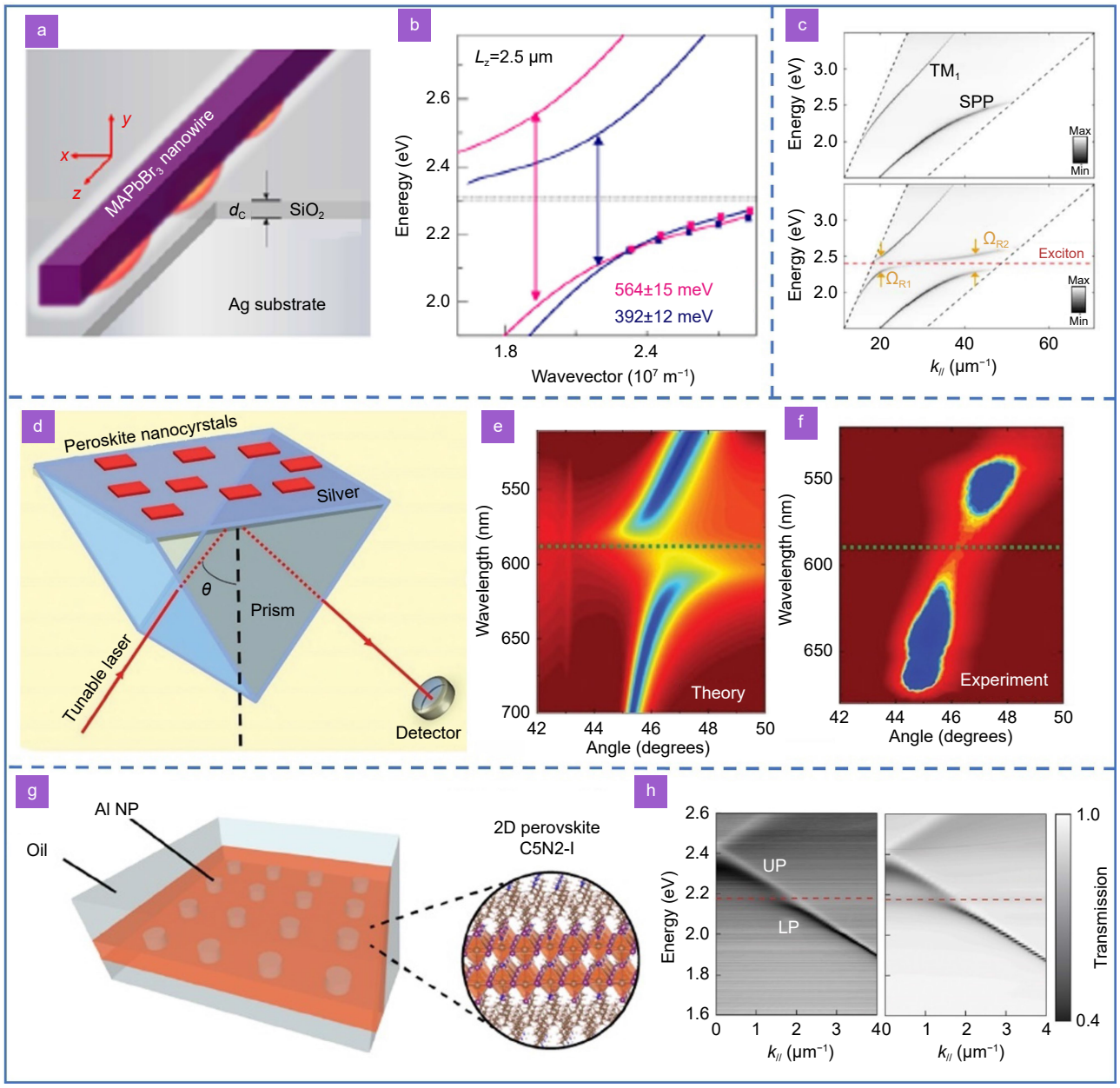


Fig. 5 | Plasmon-exciton strong coupling in perovskite. (**a**) Illustration of a hybrid plasmonic microcavity structure. (**b**) Polariton dispersion for a perovskite nanowire on top of a glass substrate (pink data points) and a SiO_2/Ag substrate (navy data points), respectively. (**c**) The angle-resolved reflectivity spectra under TM-polarization excitation of the passive and active structure indicate photonic and SPP modes in the top and bottom pales, respectively. (**d**) The Kretschmann configuration shown schematically is used for perovskite plexciton demonstration. (**e**, **f**) Perovskite plexciton dispersion curves in theory and in experiment, respectively. (**g**) Schematic drawing of $C_5N_{2\text{-}I}$ film-coated Al NP lattices, and (**h**) its experiments and finite-difference time-domain simulations of the angle-resolved transmission mapping. Figure reproduced with permission from: (a, b) ref.[53], American Chemical Society; (c) ref.[54], Chinese Laser Press; (d–f) ref.[55], Royal Society of Chemistry; (g, h) ref.[56], American Chemical Society.

ic structure is depicted schematically in Fig. 5(g). Due to the open cavity feature of the system, the coupling strength of the system was altered by altering either the superstate refractive index or perovskite thickness. Avoided crossings were seen in both experiments and finite-difference time-domain simulations of the angle-resolved transmission mapping as presented in Fig. 5(h) left and right panels, respectively. The authors have also shown that both polaritons branches have faster excited-state dynamics than pure excitons, according to ultrafast transient absorption spectroscopy measurements.

Strong coupling in perovskite enabled by dielectric nanostructures

Similar to plasmonic metasurfaces supported by plasmonic resonances, all-dielectric metasurfaces made of high refractive index semiconductors support multipolar electric and magnetic Mie resonances, thus providing an excellent platform for realizing strong light-matter interaction. On the other hand, they can be fabricated with standard nanofabrication technology. Furthermore, besides being applicable to various excitonic materials, the metasurface provides significant flexibility for modifying polaritonic features such as quality factor, group velocity, and emission pattern. As previously stated, exciton-polariton in perovskite semiconductors was first demonstrated in 1998 in a distributed feedback (DFB) microcavity[28]. The DFB cavity is created by filling a prepatterned quartz substrate with PEPI perovskite, followed by a polystyrene overcoating film. Rabi-splitting as high as 100 meV at ambient temperature is achieved by adjusting the grating period or incidence angle, which results in anti-crossing behaviour in the absorption spectrum. Few years later, organic–inorganic layered perovskite $(C_6H_5C_2H_4NH_3)_2PbI_4$ [bis-(phenethylammonium) tetraiodoplumbate (PAPI)] is strongly coupled to an ordered array of silica microspheres[29]. The authors further shown that it is possible to flexibly modify the coupling conditions of photons and excitons by adjusting the size of silica microspheres.

Recently, by using a resonant metasurface constructed from a sub-wavelength 2D lattice of perovskite pillars, Nguyen Ha My Dang et al. experimentally and theoretically demonstrated exciton-polaritons operating at room temperature[57]. The perovskite metasurface is designed by first fabricating SiO_2 holes array as backbone structure and then spin-coating PEPI in dimethylformamide (DMF) solution followed by a PMMA layer. Figure 6(a) shows the 3D schematic drawing of the proposed system. Exciton-polaritons with Rabi splitting of 200 meV are obtained in both angular-resolved PL and reflectivity experiments. Additionally, polaritonic dispersions displaying linear, parabolic, and multivalley dispersions are produced by engineering the photonic Bloch mode. Figure 6(b) depicts both the predicted absorption and the observed PL spectrum of the multivalley polaritonic mode dispersion induced by strong coupling between the PEPI exciton and an S-polarized exotic mode with a W-shaped multivalley dispersion with two off-F minima. These findings could pave the way to large-scale, inexpensive integrated perovskite polaritonic devices that operate at ambient temperature.

In a subsequent report, the strong coupling in the perovskite was optimised using a quasi-bound state in the continuum (QBIC) with a high-quality factor (*Q*-factor) to double the Rabi-splitting value while still using the same material parameters[10]. It has been determined that the maximum Rabi splitting can be increased up to a record high value of 400 meV by exploiting the extreme electric field confinement made possible by a high-*Q* mode. Two all-perovskite metagrating nanostructures supporting symmetry-protected BICs and toroidal dipole BICs were proposed in this report, as shown in Fig. 6(c) and 6(e), respectively. By either breaking the structural symmetry or tuning the distance between two identical nanowires, BICs are converted into QBICs with high *Q*-factors. The simulation results show that the enhanced strong coupling is primarily caused by the QBIC mode's *Q*-factor and the perovskite metasurface's thickness. The Rabi-splitting dependence on the *Q*-factor is shown in Fig. 6(d) as the *Q*-factor of the SB-QBIC system is tuned from 50 to 10,000. It is clear that the Rabi-splitting starts to increase sharply at low *Q*-factor values and becomes saturated at *Q* values above 800. A similar trend was observed by increasing the perovskite thickness in Fig. 6(f), which depicts the SP-QBIC system's Rabi-splitting dependence on perovskite thickness.

Later, strong coupling in 2D PEPI perovskite is theoretically and experimentally realised by leveraging BICs[58]. Figure 6(g) presents a schematic representation of the proposed structure, which was created by spin-coating PEPI and PMMA layers on a quartz substrate with a prefabricated square lattice of circular patterns. The Rabi-splitting of 205 meV was then achieved by mapping the energy of the nanostructure's reflection spectrums as a function of the in-plane wavevector k_x/k_0, as shown in Fig. 6(h). In addition, room temperature topological singularities were found after determining the Stokes parameters of PL emission in the Fourier plane. It has been found that circular patterns exhibit polarisation vortices, whereas symmetry-broken structures based on triangular patterns exhibit a large degree of circular polarisation (DCP) of 0.835. Therefore, this work suggests that active photonic devices made from polaritonic BICs based on 2D perovskite materials may have superior material characteristics as well as distinctive topological properties.

Another report further confirmed numerically and

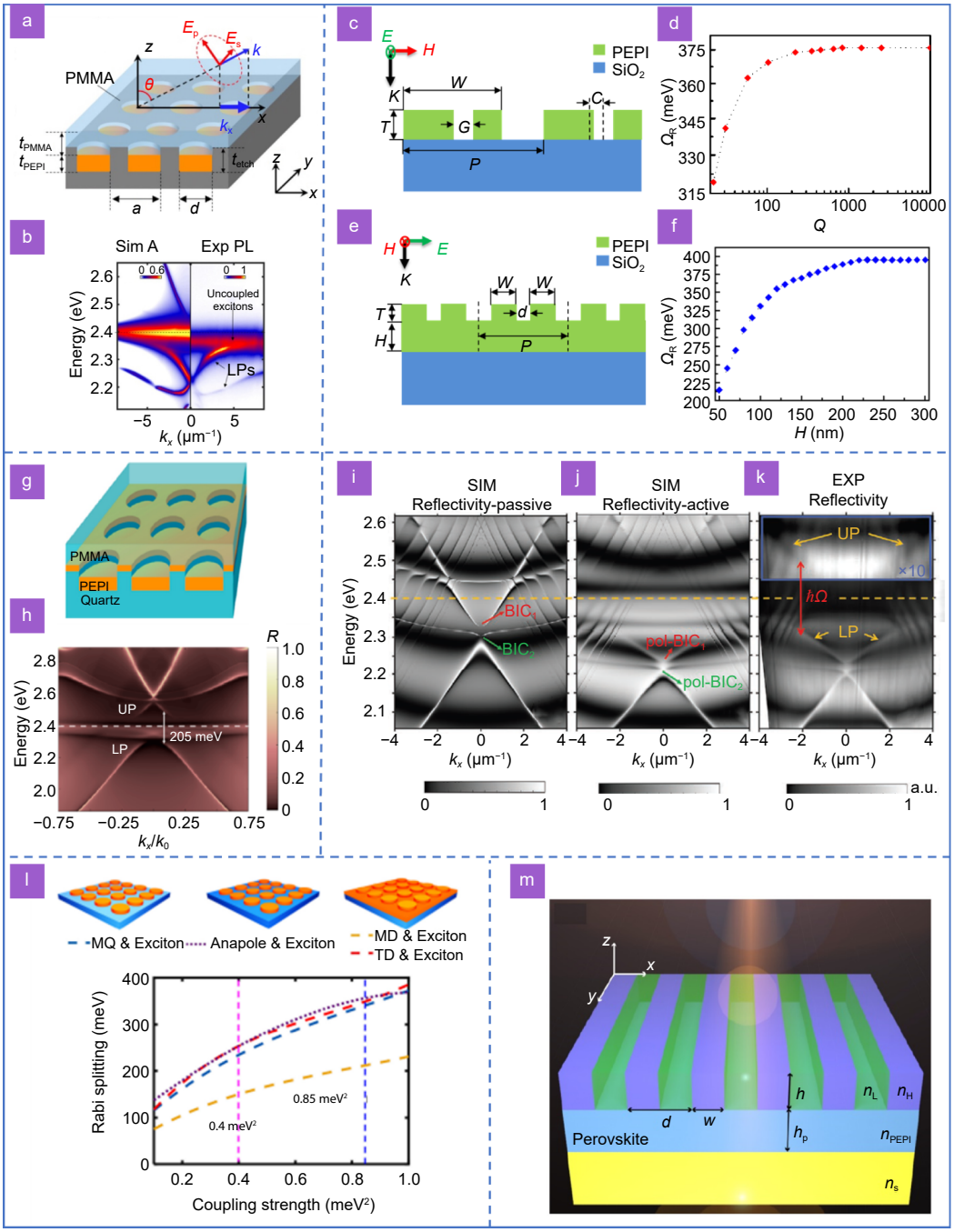


Fig. 6 | Strong coupling in perovskite using dielectric nanostructures. (**a**) Schematics for the all-dielectric circular pattern. (**b**) Comparison of numerical simulations of the angular-resolved RCWA absorption by the active structures (left panels) and experimental data (normalised) of the angle-resolved PL response (right panels). (**c**) Illustrates the 2D schematic drawing as well as the structural parameters for the SB-QBIC-based PEPI polariton system. (**d**) The Rabi-splitting reliance on the *Q*-factor of the SB-QBIC system. (**e**) Illustrates the 2D schematic diagram of the compound structure that supports SP-QBIC based on two identical NWs with continuous film underneath. (**f**) The Rabi-splitting reliance on the perovskite thickness of the SP-QBIC system. (**g**) Schematic illustration of the circular pattern. (**h**) Simulated reflection maps for strongly coupled perovskite structures. (**i**, **j**) Computed angle-resolved reflectivity spectra for the passive structure and the active structure, respectively. (**k**) The angle-resolved reflectance of the PEPI metasurface after being excited by polarised light, as measured experimentally. (**l**) Rabi splitting dependence on perovskite exciton oscillator strength, where the oscillator strength was varied from 0.1 to 1 meV² for three structures. (**m**) Illustration of the dielectric one-dimensional grating structure designed for perovskite's strong coupling. Figure reproduced with permission from: (a, b) ref.[57], American Chemical Society; (c–f) ref.[10], John Wiley and Sons; (g, h) ref.[58], American Chemical Society; (i, j) ref.[59], John Wiley and Sons; (l) ref.[60], American Physical Society; (m) ref.[61], Elsevier.

experimentally the transfer of such topological nature of the BIC photonic mode to the exciton-polariton in perovskite using a similar design[59]. The presence of two symmetry-protected BICs, designated as BIC_1 and BIC_2, is shown in Fig. 6(i), which maps the simulated reflection of the passive structures as a function of the angle of incidence. Following that, by taking active structure into account, two polaritonic branches are formed, and all dispersion curves are strongly red-shifted from the bare exciton energy, as demonstrated by the simulated reflectivity spectra shown in Fig. 6(j). These results are further supported experimentally by measuring the system's angle-resolved reflectivity spectra (Fig. 6(k)). Furthermore, polarization vortex was realized both in the bare photonic BIC and in the far field emission of the polariton BIC modes.

According to a more recent report[60], the strong coupling in perovskite could also be enhanced by a metasurface that supports multipolar Mie resonances, such as magnetic quadrupole dominant (MQ), anapole, magnetic-dipole (MD) and toroidal-dipole (TD) resonances. The strong coupling in perovskite is revealed with a Rabi-splitting of 230.7 meV in MQ resonance and 253 meV in both anapole and TD resonances using an array of perovskite nanodisks. Additionally, as shown in Fig. 6(l), the relationship between the Rabi splitting and the exciton mode's oscillatory strength was also examined, showing almost linear dependence.

More recently, dielectric grating supporting guided mode resonance (GMR) was strongly coupled to PEPI exciton in a theoretical study[61]. A 1D grating nanostructure with a refractive index of n_H =1.62 was placed on top of a PEPI perovskite film as schematically shown in Fig. 6(g). By sweeping the period of the grating, anti-crossing behaviour is realized with maximum Rabi-splitting of 378 meV. Moreover, confining light to the perovskite metasurface, utilizing the anapole modes in the perovskite metasurface, and subsequently hybridizing it with excitons in the same material could surpass a Rabi splitting of 500 meV[62]. This large Rabi splitting induced by the phenethylammonium lead iodide (PEPI) metasurface indicates the formation of self-hybridized exciton-polaritons within the metasurface.

Finally, we summarize the Rabi splitting observed in exciton-polaritons when perovskites are hybridized with different optical cavities, highlighting how the interaction strength varies with both the material and cavity type. Different perovskite compositions, such as 3D lead halide perovskites and 2D layered perovskites, exhibit varying degrees of splitting depending on their excitonic properties and the cavity's confinement effects. Optical cavities including Fabry-Pérot resonators, distributed Bragg reflectors (DBRs), dielectric metasurfaces, and plasmonic structures, enhance this coupling in distinct ways, influencing the transition from weak to strong coupling regimes. As a result, Table 1 presents a comparative analysis, demonstrating how perovskite-cavity hybrid systems can be engineered to achieve strong

Table 1 | Comparative analysis of cavity/structure types of perovskite exciton-polariton systems and their key achievements.

Cavity/structure	Perovskite system	$\hbar\Omega$ (meV)	Key achievement	Ref.
DFB microcavities	PEPI perovskite thin films	100	Achieved large splitting at room temperature in simple nanostructured geometry.	ref.[28]
DFB Microcavity	Single-crystal perovskite layer	115	Room-temperature continuous-wave perovskite low threshold polariton lasers.	ref.[49]
Plasmonic gratings	Perovskite-coated silver gratings	150	Achieved the first realization of exciton-polaritons in plasmonic -perovskite architectures.	ref.[52]
Plasmon-enhanced microcavities	$MAPbBr_3$ NW sitting on a SiO_2/Ag substrate	564	Ultra-high coupling strengths using ssurface plasmon induced localized excitation.	ref.[53]
Metagrating via QBIC	PEPI-nanowire metagrating	400	Enhanced strong coupling due to high-*Q* factor in the perovskite metagrating.	ref.[10]
BIC-based metasurfaces	2D PEPI perovskite	205	Demonstrated topological control of 2D perovskite emission in the strong coupling regime.	ref.[58]
DBR-based microcavities	2D organic-inorganic perovskite	242	Using high *Q*-factor ~ 2200 microcavity, they achieved strong coupling.	ref.[38]
DBR mirrors	$CsPbBr_3$ microplatelets	128	Room-temperature CW optically pumped polariton condensation with an ultralow threshold of ~0.53 W cm^{-2}.	ref.[50]
—	PEPI metasurfaces	553	Demonstrated room-temperature self-hybridized exciton-polaritons within the metasurface.	ref.[62]

coupling for applications in polariton lasing, quantum optics, and light-driven technologies. The table highlights that different structures exhibit varying coupling strengths, depending on their interaction with external energy sources. For instance, the $MAPbBr_3$ nanowire (NW) on a SiO_2/Ag substrate achieves the highest Rabi splitting of 564, benefiting from the synergistic enhancement provided by high optical confinement from the silver grating, while the perovskite itself functions as a Fabry-Pérot microcavity[53].

Challenges in cavity-enhanced coupling in perovskites and pathways to commercialization

Despite notable advances in exciton-polariton in perovskites, the lack of long-term stability remains a critical barrier to commercializing perovskite-based devices. To transition from small-area demonstration devices to commercially relevant platforms such as lasers, scalable deposition methods (including slot-die coating and/or chemical vapor deposition (CVD)) must be optimized to preserve the strong coupling regime while ensuring film uniformity and reproducibility. Especially, perovskite QWs present an additional challenge because their ultrathin, well-defined layers are particularly sensitive to even minor chemical or structural changes. Achieving high-quality perovskite QWs with atomically precise thickness and uniform composition is difficult, and small thickness variations can lead to inhomogeneous broadening of exciton resonances. This, in turn, undermines the strong-coupling regime necessary for pronounced cavity-enhanced effects[63]. Consequently, the layer-by-layer growth techniques used for QW fabrication must be carefully optimized to minimize defect densities.

Additionally, for robust cavity-enhanced light-matter interactions, the resonator's photonic/plasmonic mode must closely align with the excitonic transition in the perovskite. This requirement necessitates precise control over both the optical cavity and the exciton energy of the perovskite, which is sensitive to composition, strain, and layer thickness. Even slight inhomogeneities can weaken the coherent energy exchange in the system, resulting in diminished polaritonic signatures. To address these challenges, refined synthesis routes for ultra-thin perovskite layers, improved encapsulation or protective coatings to mitigate degradation, and advanced cavity engineering are crucial for achieving reproducible and stable strong-coupling phenomena. Defect control is also essential, as pinholes and grain boundaries can act as non-radiative recombination centers, reducing quantum efficiency and accelerating degradation[64]. Strategies such as defect passivation using surface ligands and interfacial engineering can improve crystallinity, suppress recombination losses, enhance charge transport, thereby improving both efficiency and stability.

Conclusions and outlooks

Conclusions

We have reviewed recent advances in both the theoretical and experimental realization of strong light-matter interactions using various optical cavities made of perovskite semiconductors and their applications. This review highlights the latest developments in perovskite research, with a particular focus on their applications in optoelectronics and the detailed study of their physical properties under strong coupling conditions. The exceptional optical and electronic properties of perovskites, combined with their relative ease of fabrication, have attracted significant interest, motivating a wide range of studies aimed at harnessing exciton-polaritons for new photonic functionalities and fundamental research in quantum and nonlinear optics. As a result, early work focused on incorporating two-dimensional perovskite materials into various optical resonators, ranging from distributed feedback structures and photonic crystals to high-Q Fabry-Pérot microcavities. This enabled robust polariton states even at room temperature. Milestones from 2006 to 2012 demonstrated strong coupling with different mirror configurations (dielectric, metals, and hybrid mirrors), setting the stage for breakthroughs such as polariton lasing in $CsPbCl_3$ nanoplatelets and coherent polariton condensation in both organic-inorganic perovskites and $CsPbBr_3$ microwires. These accomplishments underscored the readiness of perovskite microcavities for advanced polariton physics, spanning nonlinear parametric scattering and exotic exciton states such as Rydberg excitons.

Parallel efforts harnessed plasmonic nanostructures to realize strong coupling by confining electromagnetic modes at subwavelength scales. For instance, silver gratings coated with perovskite have achieved large Rabi splitting of up to 150 meV by coupling surface plasmon polaritons (SPPs) with excitons and their biexciton counterparts. Later work on perovskite nanowires on metal substrates reported enhanced splitting values exceeding

560 meV, thanks to the focused field localization at the metal-dielectric interface. Both experimental and theoretical studies further demonstrated that perovskite films on metallic substrates can simultaneously support dielectric-guided modes and SPPs, yielding large Rabi splittings in the 200–240 meV range. Recent advances include using plasmonic nanoparticle lattices to tune coupling strengths via changes to the surrounding refractive index or perovskite layer thickness, paving the way for controllable, ultrafast polaritonic interactions at the nanoscale.

Dielectric metasurfaces present another potent platform for generating exciton-polaritons in perovskites, leveraging high-*Q* resonances like Mie resonances and bound states in the continuum (BICs). Early demonstrations utilized distributed feedback microcavities with perovskite layers to achieve Rabi splittings around 100 meV, while subsequent designs involving subwavelength pillars and arrays of silica microspheres provided greater flexibility in engineering photonic bands and dispersion relations. By exploiting quasi-BICs, researchers doubled the achievable splitting to approximately 400 meV, underscoring the importance of symmetry breaking and layer thickness in optimizing coupling strength. Notably, the formation of topological singularities and polarization vortices in these structured metasurfaces demonstrates the intriguing interplay between light-matter coupling and photonic topology. Meanwhile, guided mode resonances and multipolar Mie modes push Rabi splittings above 200 meV, offering enhanced device functionality and the potential for self-hybridized exciton-polaritons.

In conclusion, perovskite semiconductors have demonstrated remarkable versatility in establishing and exploring exciton-polaritons across various platforms, such as Fabry-Pérot cavities, plasmonic nanostructures, and dielectric metasurfaces. The strong coupling regime is reliably achieved at room temperature, enabling a broad range of nonlinear and quantum phenomena. The evolution of perovskite materials for strong light–matter coupling has progressed from nanoplatelets to 1D, single-crystal, and ultimately 2D forms, each offering unique benefits such as higher exciton binding energies and improved optical stability. Early successes with nanoplatelets proved the feasibility of strong coupling and spurred the development of more complex architectures that further refine photonic and electronic properties. This incremental approach has led to continuous improvements in coupling strength and device performance, while enhancing material stability and deepening our understanding of exciton dynamics under different confinement conditions. These hybrid excitations hold promise for advancing applications such as lasers, light-emitting diodes (LEDs), and other optoelectronic devices, positioning perovskite materials at the forefront of next-generation technology.

Outlooks

On the other hand, even though remarkable progress has been made in demonstrating exciton-polaritons in perovskites with large Rabi splitting, we believe that there is still room for improvement and significant potential for future applications.

Light-matter interaction in heterostructures

There have been limited studies on cavity-enhanced light-matter interactions in perovskite quantum wells[25] with strongly bound excitons. The interaction between a microcavity and excitons in such a system, where a perovskite emitter is coupled to a resonant cavity, is described by cavity quantum electrodynamics (CQED). Furthermore, hybridizing perovskite excitons with plasmonic surface lattice resonances (SLRs)[65] can induce enhanced light-matter interactions, leading to a strong coupling regime[66,67]. Additionally, integrating SLRs with perovskite metasurfaces for strong coupling applications leverages the strengths of both materials: the extreme light confinement of SLRs and the low-loss resonances of high-*Q* dielectrics. Specifically, the high *Q*-factor resonance and ultra-low electric field confinement of an SLR combined with high refractive index perovskite metasurfaces[10] can enhance the Rabi splitting of the system. This hybrid structure opens new horizons for developing strong coupling effects at room temperature, paving the way for superior nanophotonic and tunable optoelectronic applications.

Perovskite-based light emitting diodes

Recent research has made significant strides in developing metal halide perovskites for LEDs[68]. However, challenges remain, particularly in improving these devices' external quantum efficiency (EQE). Exciton-polariton quasiparticles, which arise from the strong coupling between excitons and photons in microcavities or photonic/plasmonic structures, could potentially solve this issue. Notably, hybridizing metal halide perovskites with higher *Q*-factor plasmonic metamaterial cavities can

induce a large Rabi splitting and efficient energy exchange within the system. This strong coupling enhances the light-matter interaction, facilitating efficient energy transfer and emission. Furthermore, excitonic polarons formed through the interaction of excitons with atomic lattice vibrations (phonons) offer a promising solution to these challenges[69]. By minimizing non-radiative pathways, excitonic polarons can boost the radiative recombination efficiency of excitons, resulting in higher emission rates and improved EQE.

Low-threshold polariton laser

Placing a semiconductor gain material in appropriately designed microcavities could induce a low-threshold polariton laser in the parity-time (PT)-symmetry-protected regime. Weilu Gao and his colleagues demonstrated continuously tunable light-matter coupling strength using the polarization of light relative to the axis of single-wall carbon nanotubes (SWCNTs) placed in a mirror[70]. The system can be tuned from a PT-protected system to a symmetry-broken one, resulting in a transition from a strong coupling regime to a weak coupling regime[71]. Similarly, by placing a perovskite in microcavities, a low-threshold polariton laser could be achieved. Moreover, placing a nanowire on top of plasmonic/photonic metamaterial cavities could decrease the threshold voltage in the strong coupling regime due to efficient energy exchange[72]. A compact and energy-efficient nanoscale laser is also desirable for future on-chip manipulation. Exciton-polaritons in perovskites offer a promising solution for future on-chip lasing by enabling low-threshold, ultrafast, and energy-efficient operation. This could be realized by hybridizing perovskite gain-plasmonic cavities to decrease the total volume of the device, leading to stronger light-matter interactions and lower power consumption[73–75]. Moreover, enhancing the spontaneous emission of semiconductor emitters is a bottleneck to achieving ultrafast lasers. However, perovskites have longer response times. To solve this problem, D. A. Litvinov et al. have investigated the possible enhancement in the spontaneous emission of perovskites over the all-visible wavelength range by changing the phase of phase-change materials (PCMs). As a result, they demonstrated the reversible control of spontaneous emission of perovskites using PCMs, showing more than a 50% change in the Purcell factor with a change in the PCM phase. PCMs such as Ge-Sb-Te and SbSe are highlighted as a promising solution for enhancing the spontaneous emission of perovskites, with the ability to modulate their optical response[76].

Single-photon source and quantum computing

In the weak coupling regime, the Purcell factor (F_P) indicates the enhancement of the emitter's emission rate (γ) through the cavity. However, this relationship becomes invalid in the strong coupling regime, where the decay rate of the coupled hybrid states stabilizes at $\frac{\gamma_c+\gamma_x}{2}$, with γ_c being the decay rate of the cavity mode and γ_x the emitter's emission rate, particularly in the limit of large detuning from the cavity[66]. In the strong coupling regime, the system's dynamics are dominated by the coupling strength, $g \propto Q/\sqrt{V}$, where Q is the cavity's quality factor, and V is its optical mode volume. Moreover, the strong coupling regime offers additional benefits for achieving controllable single photon source (SPS), including the potential for photon blockade and the ability to generate more complex quantum states, which are crucial for producing streams of photons that exhibit sub-Poissonian statistics and anti-bunching[77]. Unlike classical light sources, these SPSs, which exhibit a second-order correlation function $g^2(\tau=0)\approx 0$, emits exactly one photon at a time[78]. In this regard, by varying the perovskite composition, the emission wavelength of these single photons can be tuned, enabling flexible integration into various photonic systems[79]. In quantum computing, these single photons can be used as quantum bits ("qubits") to execute computations. The exciton-polariton quasiparticles also exhibit remarkable characteristics, such as low effective mass, making them ideal for quantum computing applications. While the exploration of perovskite-based polaritons is still in its early stages, the potential for developing robust and scalable quantum computing systems is vast. Future research will likely focus on optimizing the coherence properties of polariton qubits, developing efficient methods for qubit manipulation, and integrating these components into functional quantum circuits. For instance, the recent advancements in perovskite-based active multifunctional integrated photonic devices could lead to the development of sophisticated integrated optical chips, opening new avenues in quantum computing[80]. Furthermore, the pronounced nonlinearities and high oscillator strengths in perovskite also provide a platform for polariton-based quantum simulations, allowing the exploration of complex many-body phenomena. Therefore,

future work will likely focus on refining perovskite synthesis for precise exciton energy tuning, stabilizing its quantum properties under ambient conditions, and integrating these systems with established quantum computing architectures.

Enhanced gas or particle sensors

Dielectric metasurfaces with a high *Q*-factor are highly desirable for enhancing gas or particle sensors. Ibrahim Al-Ani and his colleagues demonstrated strong coupling between the exciton of perovskite and a quasi-bound state in the continuum (QBIC) with an extremely high *Q*-factor supported by phenethylammonium lead iodide (PEPI) perovskite metagratings[10]. Additionally, Xianxin Wu and his team have demonstrated exciton-polariton condensation from BIC in all-inorganic cesium lead bromide ($CsPbBr_3$) photonic crystals fabricated using focused ion beam (FIB) milling[81]. These high *Q*-factors in perovskite metagratings and metasurfaces can increase sensitivity in detecting minute changes in the environment, which is crucial for real-time sensing. Moreover, by appropriately optimizing the incident angle, polarization angle, and geometry of dielectric metagratings and metasurfaces, exceptional points can be achieved. These points are singularities in the parameter space of a system where two or more eigenvalues and their corresponding eigenvectors coalesce, becoming degenerate. Unique to non-Hermitian systems that interact with their environment, these exceptional points facilitate energy exchange and enable enhanced gas or particle sensing[82].

References

1. Wen XL, Xiong QH. Bose-Einstein condensation of exciton polariton in perovskites semiconductors. *Front Optoelectron* **13**, 193–195 (2020).
2. Grosso G, Pietka B, Antón-Solanas C et al. Polaritonics: introduction to feature issue. *Opt Mater Express* **14**, 155–156 (2024).
3. Huang LJ, Krasnok A, Alú A et al. Enhanced light–matter interaction in two-dimensional transition metal dichalcogenides. *Rep Prog Phys* **85**, 046401 (2022).
4. Manzeli S, Ovchinnikov D, Pasquier D et al. 2D transition metal dichalcogenides. *Nat Rev Mater* **2**, 17033 (2017).
5. Kovalenko MV, Protesescu L, Bodnarchuk MI. Properties and potential optoelectronic applications of lead halide perovskite nanocrystals. *Science* **358**, 745–750 (2017).
6. Worku M, Ben-Akacha A, Blessed Shonde T et al. The past, present, and future of metal halide perovskite light-emitting diodes. *Small Sci* **1**, 2000072 (2021).
7. Wu S, F Chen ZM, Yip HL et al. The evolution and future of metal halide perovskite-based optoelectronic devices. *Matter* **4**, 3814–3834 (2021).
8. Ji KY, Anaya M, Abfalterer A et al. Halide perovskite light‐emitting diode technologies. *Adv Opt Mater* **9**, 2002128 (2021).
9. Guo XY, Han Q, Wang J et al. Optoelectronic devices of large-scale transferred all-inorganic lead halide perovskite thin films. *ACS Appl Mater Interfaces* **15**, 24606–24613 (2023).
10. Al‐Ani IAM, As'Ham K, Huang LJ et al. Strong coupling of exciton and high‐*Q* mode in all‐perovskite metasurfaces. *Adv Opt Mater* **10**, 2101120 (2022).
11. Masharin MA, Samusev AK, Bogdanov AA et al. Room-temperature exceptional-point-driven polariton lasing from perovskite metasurface. *Adv Funct Mater* **33**, 2215007 (2023).
12. Berhe AM, As'ham K, Al-Ani I et al. Strong coupling and catenary field enhancement in the hybrid plasmonic metamaterial cavity and TMDC monolayers. *Opto-Electron Adv* **7**, 230181 (2024).
13. Berhe AM, Odebowale AA, As'Ham K et al. Large Rabi splitting and Purcell factor in coupled Ag metamaterial cavity and MoS_2 monolayer. In *2024 24th International Conference on Transparent Optical Networks* 1–4 (IEEE, 2024). http://doi.org/10.1109/ICTON62926.2024.10647562.
14. Deng F, Liu HF, Xu L et al. Strong exciton–plasmon coupling in a WS_2 monolayer on Au film hybrid structures mediated by liquid Ga nanoparticles. *Laser Photonics Rev* **14**, 1900420 (2020).
15. Gao CG, You SJ, Zhang Y et al. Strong coupling between excitons and quasi-bound states in the continuum mode with stable resonance wavelength in the near-infrared region. *Appl Phys Lett* **124**, 051701 (2024).
16. Anantharaman SB, Jo K, Jariwala D. Exciton–photonics: from fundamental science to applications. *ACS Nano* **15**, 12628–12654 (2021).
17. Moxley III FI, Ilo-Okeke EO, Mudaliar S et al. Quantum technology applications of exciton-polariton condensates. *Emergent Mater* **4**, 971–988 (2021).
18. Łempicka-Mirek K, Król M, De Marco L et al. Electrical polarization switching of perovskite polariton laser. *Nanophotonics* **13**, 2659–2668 (2024).
19. Su R, Ghosh S, Liew TC et al. Optical switching of topological phase in a perovskite polariton lattice. *Sci Adv* **7**, eabf8049 (2021).
20. Masharin MA, Oskolkova T, Isik F et al. Giant ultrafast all-optical modulation based on exceptional points in exciton–polariton perovskite metasurfaces. *ACS Nano* **18**, 3447–3455 (2024).
21. Fu YP, Zhu HM, Chen J et al. Metal halide perovskite nanostructures for optoelectronic applications and the study of physical properties. *Nat Rev Mater* **4**, 169–188 (2019).
22. Miyata A, Mitioglu A, Plochocka P et al. Direct measurement of the exciton binding energy and effective masses for charge carriers in organic–inorganic tri-halide perovskites. *Nat Phys* **11**, 582–587 (2015).
23. Bouteyre P, Nguyen HS, Lauret JS et al. Room-temperature cavity polaritons with 3D hybrid perovskite: toward large-surface polaritonic devices. *ACS Photonics* **6**, 1804–1811 (2019).
24. Ouyang CX, Li Y, Fu XW et al. Room temperature exciton-polaritons in high-quality 2D Ruddlesden–Popper perovskites $(BA)_2(MA)_{n-1}Pb_nI_{3n+1}$ (n= 3, 4). *Appl Phys Lett* **117**, 221107 (2020).
25. Blancon JC, Stier AV, Tsai H et al. Scaling law for excitons in 2D perovskite quantum wells. *Nat Commun* **9**, 2254 (2018).
26. Zhang Q, Su R, Liu XF et al. High-quality whispering-gallery-mode lasing from cesium lead halide perovskite nanoplatelets.

Adv Funct Mater **26**, 6238–6245 (2016).
27. Polimeno L, Coriolano A, Mastria R et al. Room temperature polariton condensation from Whispering gallery modes in $CsPbBr_3$ microplatelets. *Adv Mater* **36**, 2312131 (2024).
28. Fujita T, Sato Y, Kuitani T et al. Tunable polariton absorption of distributed feedback microcavities at room temperature. *Phys Rev B* **57**, 12428–12434 (1998).
29. Sumioka K, Nagahama H, Tsutsui T. Strong coupling of exciton and photon modes in photonic crystal infiltrated with organic–inorganic layered perovskite. *Appl Phys Lett* **78**, 1328–1330 (2001).
30. Brehier A, Parashkov R, Lauret JS et al. Strong exciton-photon coupling in a microcavity containing layered perovskite semiconductors. *Appl Phys Lett* **89**, 171110 (2006).
31. Wenus J, Parashkov R, Ceccarelli S et al. Hybrid organic-inorganic exciton-polaritons in a strongly coupled microcavity. *Phys Rev B* **74**, 235212 (2006).
32. Lanty G, Bréhier A, Parashkov R et al. Strong exciton–photon coupling at room temperature in microcavities containing two-dimensional layered perovskite compounds. *New J Phys* **10**, 065007 (2008).
33. Pradeesh K, Baumberg JJ, Prakash GV. Strong exciton-photon coupling in inorganic-organic multiple quantum wells embedded low-Q microcavity. *Opt Express* **17**, 22171–22178 (2009).
34. Lanty G, Zhang S, Lauret JS et al. Hybrid cavity polaritons in a ZnO-perovskite microcavity. *Phys Rev B* **84**, 195449 (2011).
35. Han Z, Nguyen HS, Boitier F et al. High-Q planar organic–inorganic Perovskite-based microcavity. *Opt Lett* **37**, 5061–5063 (2012).
36. Wei Y, Lauret J, Galmiche L et al. Strong exciton-photon coupling in microcavities containing new fluorophenethylamine based perovskite compounds. *Opt Express* **20**, 10399–10405 (2012).
37. Su R, Diederichs C, Wang J et al. Room-temperature polariton lasing in all-inorganic perovskite nanoplatelets. *Nano Lett* **17**, 3982–3988 (2017).
38. Wang J, Su R, Xing J et al. Room temperature coherently coupled exciton–polaritons in two-dimensional organic–inorganic perovskite. *ACS Nano* **12**, 8382–8389 (2018).
39. Su R, Wang J, Zhao JX et al. Room temperature long-range coherent exciton polariton condensate flow in lead halide perovskites. *Sci Adv* **4**, eaau0244 (2018).
40. Bao W, Liu XZ, Xue F et al. Observation of Rydberg exciton polaritons and their condensate in a perovskite cavity. *Proc Natl Acad Sci USA* **116**, 20274–20279 (2019).
41. Fieramosca A, Polimeno L, Ardizzone V et al. Two-dimensional hybrid perovskites sustaining strong polariton interactions at room temperature. *Sci Adv* **5**, eaav9967 (2019).
42. Su R, Ghosh S, Wang J et al. Observation of exciton polariton condensation in a perovskite lattice at room temperature. *Nat Phys* **16**, 301–306 (2020).
43. Polimeno L, Fieramosca A, Lerario G et al. Observation of two thresholds leading to polariton condensation in 2D hybrid perovskites. *Adv Opt Mater* **8**, 2000176 (2020).
44. Wu JQ, Ghosh S, Su R et al. Nonlinear parametric scattering of exciton polaritons in perovskite microcavities. *Nano Lett* **21**, 3120–3126 (2021).
45. Jin F, Mandal S, Wang XT et al. Perovskite topological exciton-polariton disclination laser at room temperature. arXiv: 2404.18360 (2024). https://doi.org/10.48550/arXiv.2404.18360
46. Tao RJ, Peng K, Haeberlé L et al. Halide perovskites enable polaritonic *XY* spin Hamiltonian at room temperature. *Nat Mater* **21**, 761–766 (2022).
47. Wang TT, Zang ZH, Gao YC et al. Electrically pumped polarized exciton-polaritons in a halide perovskite microcavity. *Nano Lett* **22**, 5175–5181 (2022).
48. Bujalance C, Caliò L, Dirin DN et al. Strong light–matter coupling in lead halide perovskite quantum dot solids. *ACS Nano* **18**, 4922–4931 (2024).
49. Zou C, Cao XH, Wang ZX et al. Continuous-wave perovskite polariton lasers. *Sci Adv* **11**, eadr8826 (2025).
50. Song JP, Ghosh S, Deng XY et al. Room-temperature continuous-wave pumped exciton polariton condensation in a perovskite microcavity. *Sci Adv* **11**, eadr1652 (2025).
51. Spencer MS, Fu YP, Schlaus AP et al. Spin-orbit–coupled exciton-polariton condensates in lead halide perovskites. *Sci Adv* **7**, eabj7667 (2021).
52. Niu W, Ibbotson LA, Leipold D et al. Image excitons and plasmon-exciton strong coupling in two-dimensional perovskite semiconductors. *Phys Rev B* **91**, 161303(R) (2015).
53. Shang QY, Zhang S, Liu Z et al. Surface plasmon enhanced strong exciton-photon coupling in hybrid inorganic-organic perovskite nanowires. *Nano Lett* **18**, 3335–3343 (2018).
54. Lu LR, Le-Van Q, Ferrier L et al. Engineering a light–matter strong coupling regime in perovskite-based plasmonic metasurface: quasi-bound state in the continuum and exceptional points. *Photonics Res* **8**, A91–A100 (2020).
55. Guvenc CM, Polat N, Balci S. Strong plasmon–exciton coupling in colloidal halide perovskite nanocrystals near a metal film. *J Mater Chem C* **8**, 16520–16526 (2020).
56. Park JE, López-Arteaga R, Sample AD et al. Polariton dynamics in two-dimensional ruddlesden-popper perovskites strongly coupled with plasmonic lattices. *ACS Nano* **16**, 3917–3925 (2022).
57. Dang NHM, Gerace D, Drouard E et al. Tailoring dispersion of room-temperature exciton-polaritons with perovskite-based subwavelength metasurfaces. *Nano Lett* **20**, 2113–2119 (2020).
58. Kim S, Woo BH, An SC et al. Topological control of 2D perovskite emission in the strong coupling regime. *Nano Lett* **21**, 10076–10085 (2021).
59. Dang NHM, Zanotti S, Drouard E et al. Realization of polaritonic topological charge at room temperature using polariton bound states in the continuum from perovskite metasurface. *Adv Opt Mater* **10**, 2102386 (2022).
60. As'ham K, Al-Ani I, Lei W et al. Mie exciton-polariton in a perovskite metasurface. *Phys Rev Appl* **18**, 014079 (2022).
61. Wu J, Qing YM. Strong coupling of exciton and guided mode in perovskite film with high fabrication-tolerant scheme. *Opt Laser Technol* **155**, 108437 (2022).
62. Yang WM, Wang JY, He YL et al. Anapole assisted self-hybridized exciton–polaritons in perovskite metasurfaces. *Nanoscale* **16**, 6068–6077 (2024).
63. Eperon GE, Burlakov VM, Docampo P et al. Morphological control for high performance, solution‐processed planar heterojunction perovskite solar cells. *Adv Funct Mater* **24**, 151–157 (2014).
64. Zhang XY, Wang XB, Liu H et al. Defect engineering of metal halide perovskite optoelectronic devices. *Prog Quant Electron* **86**, 100438 (2022).
65. Kravets VG, Kabashin AV, Barnes WL et al. Plasmonic surface

lattice resonances: a review of properties and applications. *Chem Rev* **118**, 5912–5951 (2018).
66. Press D, Götzinger S, Reitzenstein S et al. Photon antibunching from a single quantum-dot-microcavity system in the strong coupling regime. *Phys Rev Lett* **98**, 117402 (2007).
67. Chikkaraddy R, de Nijs B, Benz F et al. Single-molecule strong coupling at room temperature in plasmonic nanocavities. *Nature* **535**, 127–130 (2016).
68. Li XY, Shen X, Lv QH et al. Metal halide perovskites: promising materials for light-emitting diodes. *Coatings* **14**, 83 (2024).
69. Dai ZB, Lian C, Lafuente-Bartolome J et al. Theory of excitonic polarons: from models to first-principles calculations. *Phys Rev B* **109**, 045202 (2024).
70. Gao WL, Li XW, Bamba M et al. Continuous transition between weak and ultrastrong coupling through exceptional points in carbon nanotube microcavity exciton–polaritons. *Nat Photonics* **12**, 362–367 (2018).
71. Miri MA, Alù A. Exceptional points in optics and photonics. *Science* **363**, eaar7709 (2019).
72. Liao JW, Huang ZT, Wu CH et al. Highly localized surface plasmon nanolasers via strong coupling. *Nano Lett* **23**, 4359–4366 (2023).
73. Ning CZ. Semiconductor nanolasers and the size-energy-efficiency challenge: a review. *Adv Photonics* **1**, 014002 (2019).
74. Ding K, Diaz JO, Bimberg D et al. Modulation bandwidth and energy efficiency of metallic cavity semiconductor nanolasers with inclusion of noise effects. *Laser Photonics Rev* **9**, 488–497 (2015).
75. Shi Y, Deng XY, Gan YS et al. Ten years of perovskite lasers. *Adv Mater* **19**, 2413559 (2025).
76. Litvinov DA, Kushchenko OM, Sinelnik AD et al. Enhancement of perovskite spontaneous emission by phase change materials. *J Phys D* **57**, 155103 (2024).
77. Birnbaum KM, Boca A, Miller R et al. Photon blockade in an optical cavity with one trapped atom. *Nature* **436**, 87–90 (2005).
78. Esmann M, Wein SC, Antón‐Solanas C. Solid-state single-photon sources: recent advances for novel quantum materials. *Adv Funct Mater* **34**, 2315936 (2024).
79. Sutherland BR, Sargent EH. Perovskite photonic sources. *Nat Photonics* **10**, 295–302 (2016).
80. Han Q, Wang J, Tian SS et al. Inorganic perovskite-based active multifunctional integrated photonic devices. *Nat Commun* **15**, 1536 (2024).
81. Wu XX, Zhang S, Song JP, et al. Exciton polariton condensation from bound states in the continuum at room temperature. *Nat Commun* **15**, 3345 (2024).
82. Khanbekyan M. Exceptional-point-enhanced coupled microcavities for ultrasensitive particle sensing. *Phy Rev A* **108**, 023710 (2023).

Acknowledgements

This work is supported by the Australian Research Council (DP200101353).

Competing interests

The authors declare no competing financial interests.

Scan for Article PDF